Rare Metal Materials and Engineering
Volume 54, Issue 8, August 2025
Available online at www.rmme.ac.cn

Science Press

Cite this article as: Li Yan, Wang Guicheng, Zhang Wenbin, et al. Microstructure and Mechanical Properties of Explosively Welded Nickel/Steel Composite Plate Interface[J]. Rare Metal Materials and Engineering, 2025, 54(08): 1971-1979. DOI: https://doi.org/10.12442/j.issn.1002-185X.20240350.

ARTICLE

Microstructure and Mechanical Properties of Explosively Welded Nickel/Steel Composite Plate Interface

Li Yan[1,2], Wang Guicheng[1], Zhang Wenbin[1], Yang Haijuan[1], Li Jucai[2], Liu Cuirong[1,2]

[1] School of Material Science and Engineering, Taiyuan University of Science and Technology, Taiyuan 030024, China; [2] School of Intelligent Manufacturing Industry, Shanxi University of Electronic Science and Technology, Linfen 041000, China

Abstract: High-performance pure nickel N6/steel 45# composite plate (N6/45#) was prepared using explosive welding technique. The microstructure of the interface and nearby regions was characterized and analyzed by optical microscope, scanning electron microscope, electron backscatter diffraction, and mechanical property testing, and the microstructural features and mechanical properties of the explosive welding interface were explored. The results show that along the direction of explosive welding, the pure nickel N6/steel 45# composite plate interface gradually evolves from a flat bond to a typical wavy bond. The grains at the crests and troughs exhibit high heterogeneity, and the closer to the interface, the finer the grains. Recrystallization and low-stress deformation bands are formed at the bonding interface. Nanoindentation tests reveal that plastic deformation occurs in the interfacial bonding zone, and the nanohardness values in the crest regions are higher than that in the trough regions. The tensile strength of the N6/45# interface is 599.8 MPa, with an average shear strength of 326.3 MPa. No separation phenomenon is observed between N6 and 45# after the bending test.

Key words: explosive welding; pure nickel N6/steel 45# composite plate; microstructure; nanoindentation

1 Introduction

Explosive welding is a method for joining dissimilar materials using detonation waves as the driving force. This method offers notable advantages such as a small heat-affected zone and a stable bonding interface[1]. Widely used in the production of metal composite plates, explosive welding enables high-strength bonding between dissimilar metals with significantly different properties, and successfully produces various high-performance metal composite plates. Zhang et al[2] used explosive welding to prepare copper/stainless steel composite plates by varying explosion ratios, obtaining the desired composite plates. Wang et al[3] conducted experimental and theoretical studies on the bonding interface formation, microstructure evolution, and interface strength of AA6061/AZ31B alloy composite plates prepared by explosive welding. They found that the shear strength of the bonding interface of the explosively welded AA6061/AZ31B composite plates could reach up to 201.2 MPa.

Currently, the preparation of composites is developed towards lightweight and functional materials, while also maintaining a certain level of strength and stiffness. Composite materials such as AZ31B/TA2[4] and Ti/steel[5] have been successfully fabricated. Pure nickel N6 has excellent chemical stability and corrosion resistance, which differs significantly from steel in physical properties. However, nickel/steel composites are widely used in fields such as shipbuilding and marine pipelines, making the study on nickel/steel composites particularly important[6–7]. The bonding interface, as a key area for evaluating the performance of composites, has become a focus of investigation in the field of composite material research.

In this study, pure nickel N6 and medium-carbon steel 45# were joined via explosive welding. The bonding interface of

Received date: July 09, 2024
Foundation item: Natural Science Foundation of Shanxi Province (202203021221149); Key Research and Development Program of Shanxi Province (202302010101006, 202202150401016); Scientific Research Start-up Fund for the Introduction of Talents in Shanxi Institute of Electronic Science and Technology (2023RKJ021); Key R&D Program of Linfen City (2334)
Corresponding author: Li Yan, Ph. D., Professor, School of Materials Science and Engineering, Taiyuan University of Science and Technology, Taiyuan 030024, P. R. China, E-mail: 2018023@tyust.edu.cn

the explosively welded composite plate was characterized using scanning electron microscope (SEM) equipped with an energy dispersive spectrometer (EDS), and electron backscatter diffraction (EBSD) to analyze the bonding morphology and microstructure. Nanoindentation technology was employed to test the hardness of the explosive welding interface at the nanoscale. Mechanical properties of the composite material interface were determined through stretching, bending, and shearing experiments.

2 Experiment

The composite plate used in the experiment was pure nickel N6, with dimensions of 300 mm×300 mm×1 mm. The substrate steel 45# had dimensions of 300 mm×300 mm×3 mm. The chemical composition of nickel N6 and steel 45# is shown in Table 1.

In the explosive welding experiment, a parallel installation method was used, with the detonation initiated from the center of the edge. Before welding, the surfaces of the base and composite plates were polished and cleaned to achieve a smooth and flat surface. ANFO explosives were used, with an explosive density of 850 kg/cm³ and a theoretical detonation velocity of 2100 m/s. The spacing between the base and composite plates was 2 mm, and the charge ratio was 0.9. A schematic diagram of the explosive welding process is shown in Fig. 1. After explosive welding, the composite plates were air-cooled, and ultrasonic testing was conducted on the pure nickel N6/steel 45# composite plate (referred to as N6/45#) using ultrasonic flaw detection methods.

The microstructure of N6/45# composite plates was characterized by optical microscope (OM), scanning electron microscope (SEM) equipped with an energy dispersive spectrometer (EDS), and electron backscatter diffraction (EBSD) analysis. Nanoindentation was used to determine the nano-hardness distribution at the interface. The mechanical properties of the composite plate bonding interface were obtained through tensile, bending, and shear tests. Fig.2 shows the schematic diagrams of the tensile, bending, and shear samples.

Table 1 Chemical composition of steel 45# and nickel N6 used in the experiment (wt%)

Material	C	Si	Mn	Ni	Cu	Fe
45#	0.42	0.27	0.52	0.02	0.02	Bal.
N6	0.01	0.11	0.03	Bal.	0.008	0.05

Fig.1 Schematic diagram of explosion welding process

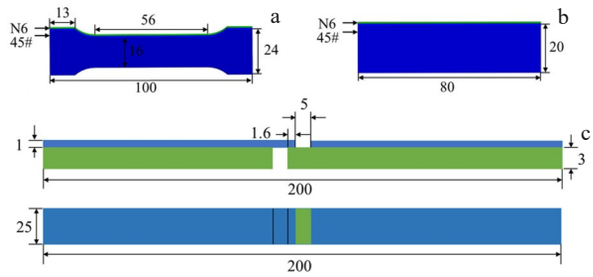

Fig.2 Schematic diagram of tensile sample (a), bending sample (b), and shear samples (c)

3 Microstructural Characterization of N6/45# Explosive Welding Interface

3.1 Interface bonding mechanism

Fig.3 shows the bonding morphology of the interface in the direction of detonation wave propagation for the N6/45# composite plate, with the upper part being the N6 side and the lower part being the 45# side. Near the initiation point, the two materials do not achieve bonding at the interface, resulting in a boundary effect. The primary reason is that during explosive welding, the detonation wave, upon reaching the boundary of the composite plate, is affected by rarefaction waves, leading to a reduction in bonding pressure. Yang et al[8] analyzed the bonding mechanism from an energy perspective through numerical simulation of explosive welding of metals, and found similar patterns. They suggested that extending the length of the composite plate can reduce the unbonded area. Additionally, at the initial stage of the explosion, the just-ignited explosive cannot produce a stable detonation wave, which can also lead to the phenomenon mentioned above. As the detonation wave is continuously propagated, a flat bond appears at the interface, which then transforms into a stable wavy interface. The appearance of the wavy interface signifies the success of explosive welding. The specific mechanism of the wavy interface has long been an important topic in the research field of explosive welding. However, no single result has been universally accepted, with two main theories including the vortex mechanism[9] and the fluid instability mechanism[10].

Fig. 4a shows the vortices at the bonding interface of the composite plate. Vortices generally form at the interface of the composite plate during explosive welding. The primary reason is that explosive welding is a rapid process, and there is a velocity difference between the fluid of the composite plate and the fluid of the substrate. The relative sliding of these two

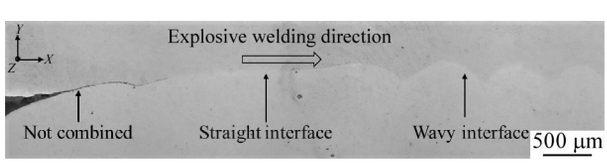

Fig.3 Interface morphology of N6/45# composite plate along the detonation direction

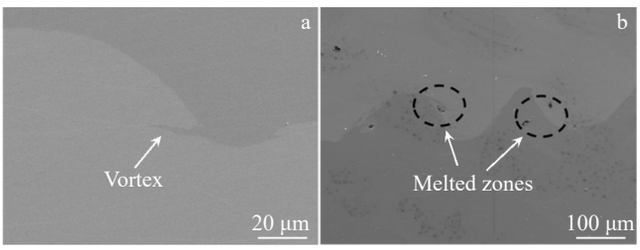

Fig.4 Interface morphologies of vortex (a) and melted zone (b)

fluids at the interface generates vortices. Fig. 4b shows the melted zones formed at the interface. It can be observed that the melted zones mainly exist on the steel 45# side, due to the relatively lower melting point of steel 45# compared to that of pure nickel N6. Although the presence of molten material can reduce the bonding strength of the composite plate interface, the bonding between metals mainly relies on elemental diffusion and plastic deformation. The presence of melted zones indicates that local melting occurs at the interface, forming intermetallic compounds during rapid cooling and solidification[11–12].

3.2 Interface element distribution

The composite plate is composed of two types of metal plates, and there is certainly a concentration difference of elements at the bonding interface. Under the influence of the detonation wave, atoms will undergo mutual diffusion[13–14]. Fig.5a shows the line scanning path (white line) at the crest of the bonding interface of the N6/45# composite plate, and Fig. 5b shows the corresponding line scanning results. The diffusion curve of elements Fe and Ni at the interface of the N6/45# composite plate is X-shaped, indicating that the mutual diffusion of the two elements occurs in the process of explosion welding. Meanwhile, it is observed that metal melts in Fig. 5a are similar to that in Fig. 4b, indicating that metallurgical bonding has occurred in the region near the interface. Furthermore, given that the atomic radii of Ni and Fe are highly similar, the explosion welding process is instantaneous (approximately 10^{-6} s) [15]. This duration is insufficient for a thick diffusion layer to form, meaning that there is no significant difference in the diffusion rates of elements Ni and Fe, and the diffusion region is narrower. No significant transition layer or stepped feature is observed in the line scanning results at the interface, suggesting that there is no continuous compound formed by metal reaction at the interface[16–17]. Table 2 shows the EDS results of the local points at the interface marked in Fig. 5. The results demonstrate that the chemical composition of points 1 and 2 is analogous to the chemical composition of steel 45#. Furthermore, the chemical composition of points 4 and 5 is similar to that of nickel N6, whereas the chemical composition of point 3 is intermediate. A thin diffusion layer appears near the interface[17], obtaining conclusions consistent with the line scanning results.

Additionally, there is a significant difference in the degree of diffusion of the two elements at the crest and trough, with

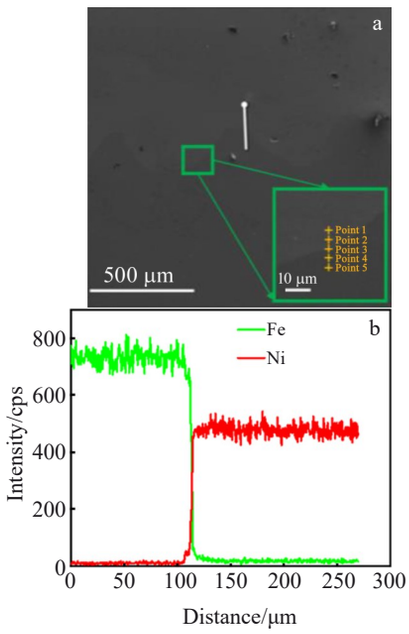

Fig.5 Near-interface peak line scanning analysis: (a) line scanning path and (b) line scanning result

Table 2 Chemical composition of points near interface as marked in Fig.5a (wt%)

Point	Fe	Mn	Si	Ni
1	99.30	0.47	0.21	0.02
2	99.28	0.52	0.18	0.02
3	10.38	0.58	0.34	88.70
4	3.45	0.18	0.21	96.16
5	0.06	0.04	0.10	98.00

the diffusion range being significantly more extensive at the crest. This is because the diffusion of elements is directly related to the driving force and diffusion mode. During explosive welding, the degree of plastic deformation at the crest is greater, resulting in a large number of vacancies and dislocations, which facilitate atomic diffusion.

Fig. 6 shows the EDS elemental mapping of elements Fe and Ni at the crests and troughs, where red represents the element Fe and green represents the element Ni. The element

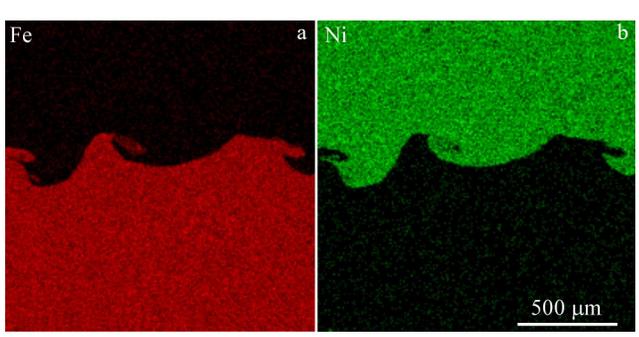

Fig.6 Near-interface EDS elemental mapping on the 45# side (a) and on the N6 side (b)

diffusion at the interface exhibits a wavy pattern, consistent with the microstructural morphology. The observed vortex phenomenon is detrimental to the stability of the interface.

3.3 EBSD analysis of interface

3.3.1 Inverse pole figure analysis of interface

Fig. 7 shows the inverse pole figure (IPF) maps of different positions of the N6/45# explosive welded composite plate. In the IPF maps, grains with different orientations are shown in different colors: red represents <001> , green represents <101> , and blue represents <111> . The black dashed line marks the boundary between the crests and troughs. It can be seen from Fig.7a that the Ni grains near the interface at the crest position are significantly smaller than Fe grains. The grain size increases with distance from the interface, showing an uneven distribution of grain sizes. The grain size statistics are shown in Fig. 7b and 7c, where the average grain size of Ni at the crest is 5.3 μm, and that of Fe is 7.74 μm. The grains far from the interface are less affected by the interface heat, maintaining their original size[18]. Fig.7e and 7f show that the average grain size of Fe at the trough is 7.25 μm, while that of Ni is 4.7 μm. The grains at the crest are larger than that at the trough, and the grains are visibly elongated in a direction parallel to the interface, suggesting that there is internal stress at the crest and trough of the interface. The internal stress is caused by the uneven phase transformation, uneven plastic flow, and cold deformation under the influence of the detonation wave at the interface.

3.3.2 Kernel average misorientation analysis

To further verify the stress distribution at the interface, kernel average misorientation (KAM) values were calculated by applying a maximum misorientation of 5° to adjacent grains, which reveals the local strain distribution in different parts of the explosive welding interface[19]. Different KAM values are typically represented by different colors: blue indicates low KAM values, green indicates moderate KAM values, and red indicates high KAM values. Generally, higher KAM values indicate greater local stress. The crest and trough positions of the explosive welding interface were tested, as shown in Fig. 8. It can be seen that the plastic strain concentration areas, at the crest or the trough, exhibit a wavy pattern, indicating that significant pressure and plastic deformation occur on both sides of the interface, and thus forming a blue low-plastic deformation band at the bonding interface. The stress concentration at the trough is significantly lower than that at the crest and it appears as a wide band.

3.3.3 Analysis of recrystallized grain distribution

To further explore the mechanism behind the differences in grain size at the crest and trough in Fig. 7, the distribution of recrystallized grains at these positions was analyzed. Fig. 9 shows the characteristics and proportion statistics of grains at the crest and trough of the N6/45# composite plate bonding interface. Due to the varying distances from the interface, the effect of the detonation wave decreases gradually with increasing distance from the interface, which is consistent with the grain size distribution patterns in Fig. 7a and 7b. In Fig.9a, blue represents recrystallized grains, yellow represents substructure grains, and red represents deformed grains. In Fig. 9a, the Ni side consists of 52.2% substructure grains, 15.4% deformed grains, and 32.4% recrystallized grains. The Fe side consists of 64.0% deformed grains, 6.1% recrystallized grains, and 31.9% substructure grains. In Fig.9b, the Ni side consists of 71.7% recrystallized grains, 24.9%

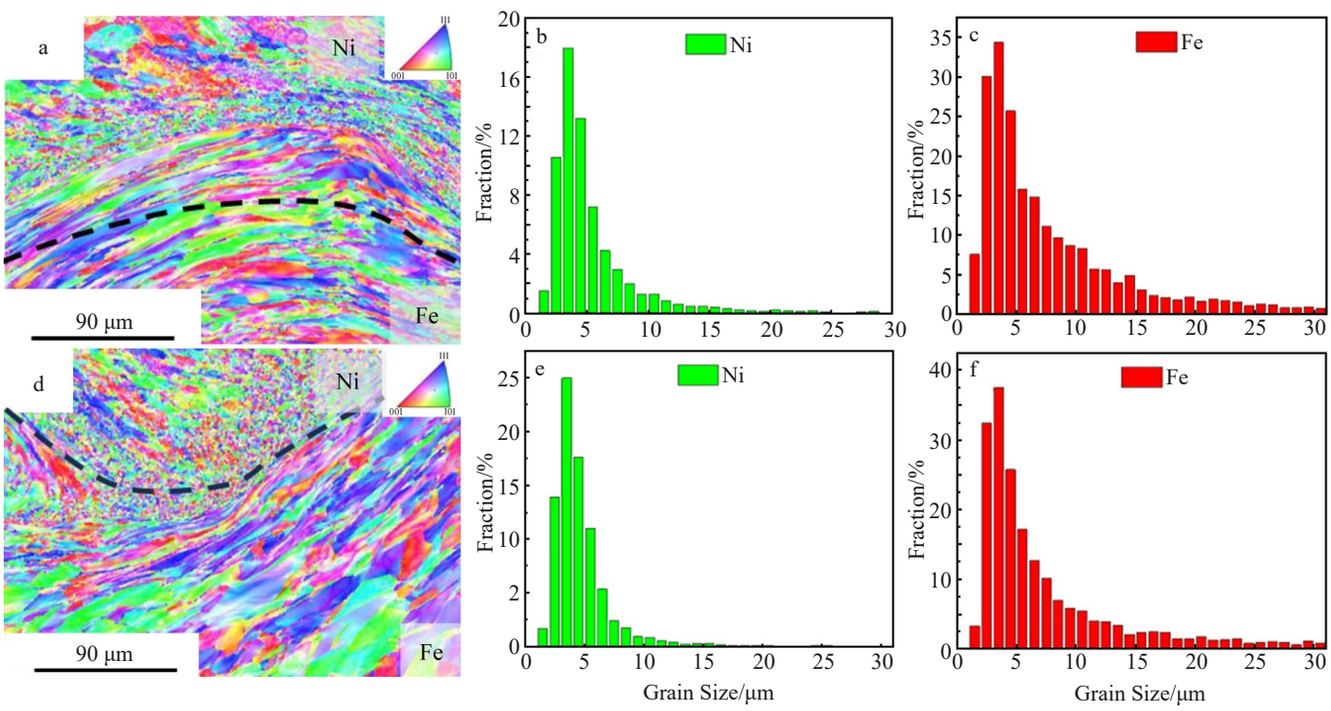

Fig.7 IPF maps of N6/45# explosive welding composite plate (a, d) and grain size distribution of elements Ni (b, e) and Fe (c, f) at different locations: (a–c) crest and (d–f) trough

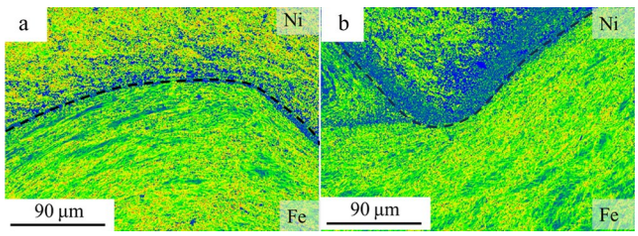

Fig.8 KAM maps of different regions at explosive welding interface: (a) crest and (b) trough

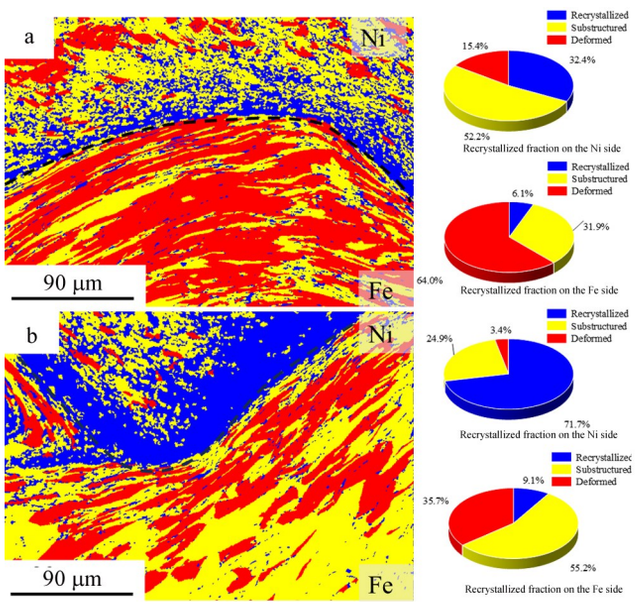

Fig.9 Grain distribution characteristics and proportion statistics at the crest (a) and trough (b) of the composite plate

substructure grains, and 3.4% deformed grains. Under the action of the detonation wave, grains undergo varying degrees of transformation from plastically deformed grains to substructure grains, and then to recrystallized grains. From Fig.9a, it can be seen that the grains near the interface on the Ni side are mainly fine recrystallized grains, and as the distance from the interface increases, the grains gradually become substructure grains and deformed grains. The recrystallization process leads to a certain degree of grain refinement[20–21]. This also reflects the phenomenon of increased grain size on the Ni side due to reduced undercooling and uneven plastic deformation. On the Fe side of the interface, the grains are in the form of deformed grains and substructure grains. This is because when the detonation wave reaches the Fe side, after plastic deformation occurs, the detonation wave energy is insufficient to reach the recrystallization temperature. The grains on the Fe side undergo dislocation slip and grain deformation under the action of plastic deformation, resulting in the presence of deformed grains and substructure grains. In Fig.9b, the Fe side undergoes a similar process as that in Fig. 9a, while a broad band of recrystallized grains appears on the Ni side of the interface. Recrystallized grains help to reduce strain, which corresponds to the grain refinement and low-stress bands observed in Fig. 9b and 9c, indicating that recrystallization occurs at the trough during explosive welding. The high strain is released, and recrystallized grains are refined. Similar phenomena are also observed in Ti/Ni, Ti/Fe, and other materials[22–23].

3.3.4 Grain boundary distribution map

To further study the microstructure at the crests and troughs, the grain boundary distribution at these positions was analyzed. Fig. 10 shows the grain boundary distribution maps for different regions of the interface, as well as the statistical charts of high-angle grain boundaries (HAGBs) and low-angle grain boundaries (LAGBs). From Fig. 10a, it can be seen that the crest interface is primarily dominated by blue HAGBs, while most grain boundaries far from the interface are LAGBs. In Fig. 10b, the regions of HAGBs and LAGBs in the trough are similar to that in the crest, but the content of HAGBs in the trough is relatively higher. This is because, during explosive welding, the Ni side is closer to the explosive and is subjected to a greater impact force at the trough, resulting in a higher degree of plastic deformation, which also promotes recrystallization and thus leads to grain refinement, increasing the content of LAGBs on the Ni side at the trough. The Fe side shows the opposite trend.

4 Mechanical Properties

4.1 Nanoindentation analysis

Nanoindentation tests were conducted on the crests and troughs near the interface of the composite plate to analyze the nanohardness changes at the interface. Fig. 11a shows the results of the nanoindentation tests, where the nanohardness at any position in the trough is lower than that at the crest. This indicates that the strengthening effect at the crest is higher than at the trough, which is consistent with the previous results of grain boundary distribution and local stress distribution. Fig. 11b presents the load-displacement curves at different positions near the interface. Fig. 11c and 11d show the nanohardness values and elastic modulus values in different regions at the crests and troughs, respectively. Under the same maximum indentation load, the indentation depth at the crest on the steel 45# side is the smallest, and the indentation depth at the trough on the N6 side is the largest. The indentation depth at the bonding interface is between that of the two base materials. This is mainly due to the varying degrees of plastic deformation and work hardening of the materials at the interface after explosive welding, with the strengthening effect being significantly stronger at the crest. The nanohardness value at the crest region of the interface is 3.39 GPa, which is significantly higher than the 2.84 GPa at the trough, further indicating that the crest experiences a stronger strengthening effect due to explosive welding. When the material is subjected to explosive impact, high temperatures and high pressures are generated, leading to significant plastic flow and cold deformation on the material

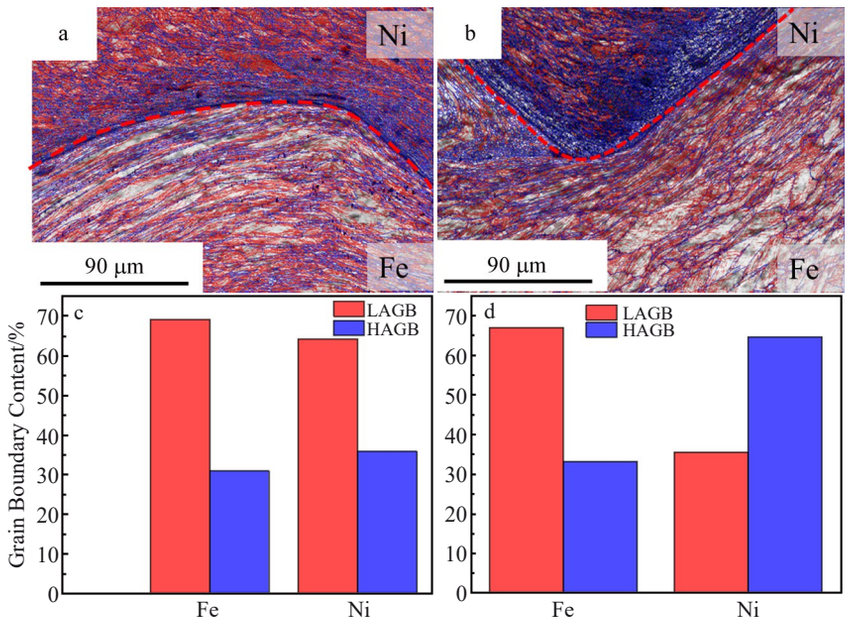

Fig.10 Distribution maps (a–b) and statistical charts (c–d) of grain boundaries at the crest (a, c) and trough (b, d)

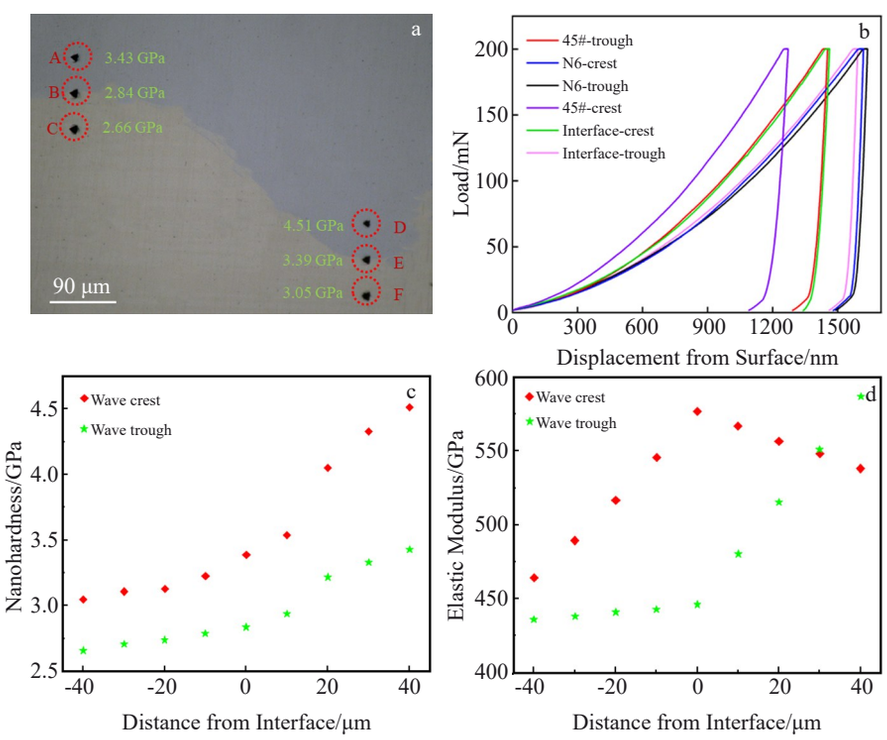

Fig.11 Nanoindentation test results (a) and load-displacement curves (b) of the bonding interface of the N6/45# composite plate after explosive welding; nanohardness (c) and elastic modulus (d) as a function of distance from the interface

surface[24]. This deformation results in a higher cooling rate and stress concentration at the crest, thus leading to higher nanohardness at the crest. In contrast, the cooling rate at the trough is relatively lower, and it experiences less stress concentration, resulting in relatively lower nanohardness at the trough.

4.2 Tensile properties of interface

To further investigate the mechanism of the influence of microstructure on mechanical properties, tensile tests and fracture morphology analyses were conducted. The impact of microstructure on mechanical properties was discussed. Table 3 shows the results of the tensile tests. The tensile strength of

Table 3 Results of tensile test of N6/45# composite plate

Yielding strength/MPa	Tensile strength/MPa	Elongation/%
495.7	599.8	12.74

the N6/45# interface is 599.8 MPa.

Fig. 12 shows the stress-strain curve, indicating that the sample underwent three stages during tensile testing: elastic deformation, plastic deformation, and fracture. To investigate the fracture mechanism of the samples, SEM analysis was conducted on the fracture surface. Fig. 13 shows the morphologies of the tensile sample. It can be seen from Fig. 13a that the N6/45# composite plate experiences slight necking, and no significant cracking is found between the base plate and the composite plate, with a relatively neat fracture surface. This is because the two materials have similar mechanical properties, resulting in comparable degrees of plastic deformation in the base plate and composite plate under the same tensile stress. As the tensile stress increases, the external tensile force exceeds the interface bonding strength, causing the tensile sample to fracture perpendicular to the interface, as shown in the figure. As shown in Fig. 13c, the microstructure of the fracture surface on the N6 side was observed through scanning, revealing many parallel strip structures, indicating that the N6 side underwent typical cleavage fracture. Observing the fracture morphology on the 45# side in Fig. 13d, the fracture surface consists of dimples with various sizes. During explosive welding, the N6 side absorbed most of the energy, leading to work hardening, while a small portion of the energy was transmitted to the 45# side, resulting in different fracture morphologies on the tensile sample.

4.3 Shear properties of interface

Considering that the load form in the shear test is similar to the service environment of the composite plate, three sets of experiments were designed to obtain more accurate performance indicators. The measured data are shown in Table 4, and Fig. 14 shows the shear strength test result, with the average shear strength of 326.3 MPa. Since the bonding interface of the composite plate is wavy, the actual bonding area is larger than the sample area, so the actual shear strength of the composite plate should be slightly lower than the calculated value, which is superior to other composite materials[25].

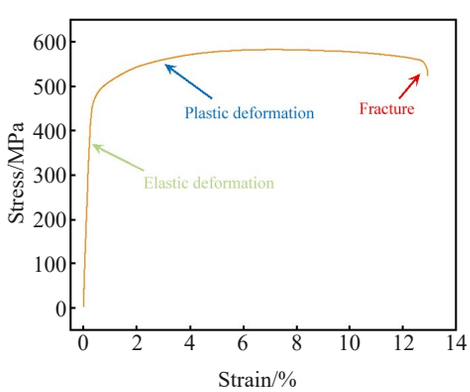

Fig.12 Stress-strain curve of N6/45# composite plate

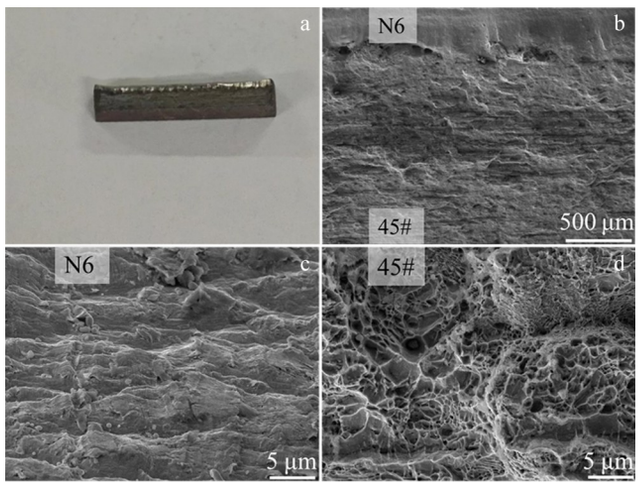

Fig.13 Tensile fracture morphologies: (a) macroscopic morphology, (b) combined interface, (c) N6 side, and (d) steel 45# side

Fig. 15 shows the morphologies of the shear fracture surface. Fig. 15a shows the macroscopic morphology of the shear fracture, where the N6/45# composite plate exhibits typical shear characteristics, including clear shear lips and angles, parallel shear stripes, and grain slip traces. The smooth shear fracture morphology is usually associated with ductile failure, indicating that the material can absorb a significant amount of energy under shear stress, exhibiting a certain degree of ductility. As shown in Fig. 15c, the microstructure of the fracture surface on the N6 side reveals regular, neat, and smooth characteristics, which are indicatives of typical cleavage fracture. Fig. 15d shows the shear fracture morphology on the 45# side, where many dimples with varying sizes are observed at the tear site, and the distribution of dimples is relatively chaotic. The presence of dimples can induce stress concentration in the depressions, reducing the peak stress, helping to slow down the crack propagation rate, and thereby delaying the material's failure.

4.4 Bending properties of interface

After the preparation of the composite plate, the delamination phenomenon under bending load is also a key indicator of the composite plate's performance. Two sets of tests were designed, i.e. internal bending and external bending, to investi-

Table 4 Results of shear test

Sample No.	Substrate thickness/mm	Composite plate thickness/mm	Bonding area/mm^2	Maximum pressure/kN	Shear strength/MPa
1	3	1	40	12.74	318.6
2				13.02	325.5
3				13.40	334.9
Average				13.05	326.3

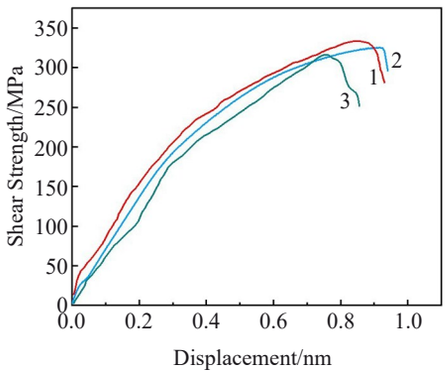

Fig.14 Test results of shear strength of three samples

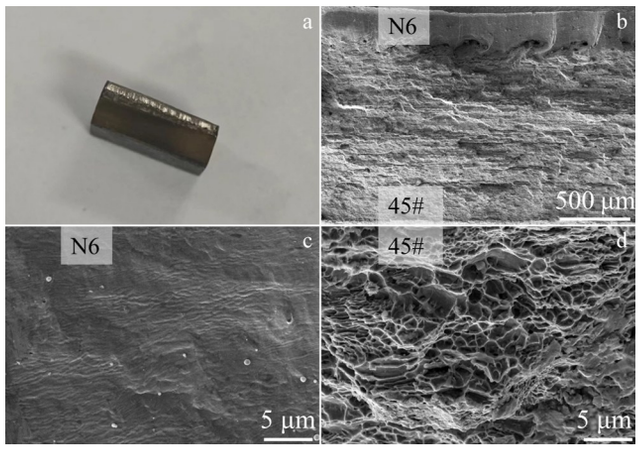

Fig.15 Shear fracture morphologies: (a) macroscopic morphology, (b) interface, (c) N6 side, and (d) steel 45# side

gate the delamination near the interface of the composite plate under bending loads in different directions. The bending test data for the N6/45# composite plate are shown in Table 5. After internal and external bending tests on the N6/45# composite plate, the bonding morphology at the interface was observed, as shown in Fig.16. It can be found that there is no separation or partial separation between the base plate and the composite plate, and the bonding interface remains intact without cracks. Fig. 17 shows the bending stress-strain curves under internal and external bending load of the composite plate.

Table 5 Statistical data of bending

Set	Length/mm	Thickness/mm	Indenter diameter/mm	Bending angle/(°)	Interface condition
Internal bending	80	4	20	120	No delamination
External bending	80	4	20	120	No delamination

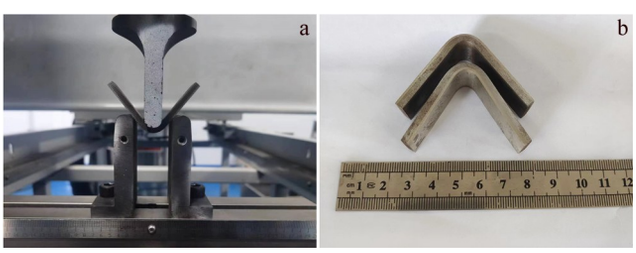

Fig.16 Bending process (a) and inner and outer bending profiles (b)

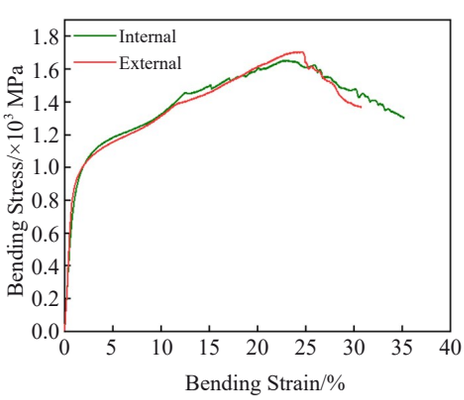

Fig.17 Stress-strain curves under internal and external bending tests

5 Conclusions

1) The explosively welded N6/45# composite plate does not achieve bonding at the initiation point due to the influence of the explosive rarefaction wave, resulting in a boundary effect. Along the detonation direction, the interface morphology is transitioned from a flat bond to a stable wavy bond, and vortex structures form at the bonding interface of the composite plate.

2) The SEM morphology and EDS results of the region near the N6/45# explosion welding bonding surface show that N6 and steel 45# form a metal composite during the explosion welding process, achieving metallurgical bonding at local area. Elements Fe and Ni diffuse with each other in the bonding area, the diffusion distance is about 1 μm. The diffusion curves of the two elements present an X-shape, the mutual diffusion of the elements improves the bonding strength at the interface, and the connection mechanism of the interface is local metallurgical bonding and mechanical bonding.

3) The grains at the interface are highly heterogeneous due to the influence of explosive welding, and the closer to the interface, the smaller the grain size. The Ni side shows a significant preferred orientation in the <111> direction, forming a blue low-stress deformation band at the bonding interface.

4) The materials in the bonding zone experience work hardening, and the nanohardness values in the trough region are higher than that in the crest region. The actual tensile strength of the N6/45# composite plate is 599.8 MPa, and the

shear strength reaches 326.3 MPa. After internal and external bending tests, no separation occurs between the base plate and the composite plate, and the bonding interface remains intact.

References

1 Sherpa Bir Bahadur, Rani Reetu. *Journal of Alloys and Metallurgical Systems*[J], 2024, 6: 100078

2 Zhang Bingyuan, Ma Honghao, Xu Junfeng *et al. Fusion Engineering and Design*[J], 2022, 179: 113142

3 Wang Huhe, Li Xiaojie, Wang Yuxin *et al*. *Journal of Materials Research and Technology*[J], 2023, 25: 7376

4 Wu Jiaqi, Wang Wenxian, Cao Xiaoqing *et al. Rare Metal Materials and Engineering*[J], 2017, 46(3): 640

5 Zu Guoyin, Sun Xi, Zhang Jinghua. *Rare Metal Materials and Engineering*[J], 2017, 46(4): 906

6 Lipińska Marta, Ura-Bińczyk Ewa, Mróz Sebastian *et al. Journal of Manufacturing Processes*[J], 2023, 105: 84

7 Zhang Conghui, Song Congbin, Zhu Wenguang *et al. Journal of Materials Research and Technology*[J], 2022, 19: 314

8 Yang Ming, Zhang Bingyuan, Ma Honghao *et al. Transactions of Nonferrous Metals Society of China*[J], 2024, 34(5): 1588

9 Li Bowen, Zhang Min, Zhang Keren *et al. Materials Letters*[J], 2024, 367: 136593

10 Ma Yong, Wang Tao, Wang Guoping *et al. Materials Today Communications*[J], 2023, 36: 106880

11 Lipińska Marta, Ura-Bińczyk Ewa, Mróz Sebastian *et al. Journal of Manufacturing Processes*[J], 2023, 105: 84

12 Mendes R, Ribeiro J B, Loureiro A. *Materials & Design*[J], 2013, 51: 182

13 Ma Yong, Zhang Song, Wang Tao *et al. Materials Today Communications*[J], 2022, 31: 103552

14 Gurevich Leonid M, Shmorgun Viktor G, Bogdanov Artem I *et al. Materials Today: Proceedings*[J], 2019, 19: 1904

15 Zhang Linjie, Pei Qiang, Zhang Jianxun *et al. Materials & Design*[J], 2014, 64: 462

16 Song J, Kostka A, Veehmayer M *et al. Materials Science and Engineering A*[J], 2011, 528(6): 2641

17 Ali Nassiri, Tim Abke, Glenn Daehn *et al. Scripta Materialia*[J], 2019, 168: 61

18 Yang Ming, Wang Jinxiang. *Journal of Materials Research and Technology*[J], 2024, 30: 4654

19 Li Ning, Zhang Min, Ye Jianlin *et al. Journal of Manufacturing Processes*[J], 2021, 64: 455

20 Gloc Michal, Wachowski Marcin, Plocinski Tomasz *et al. Journal of Alloys and Compounds*[J], 2016, 671: 446

21 Yang Ming, Xu Junfeng, Ma Honghao *et al. Composites Part B: Engineering*[J], 2021, 212: 108685

22 Bataev I A, Lazurenko D V, Tanaka S *et al. Acta Materialia*[J], 2017, 135: 277

23 Zhou Qiang, Lu Honghong, Lan Xuke *et al. Journal of Materials Research and Technology*[J], 2023, 25: 6472

24 Zhang Tingting, Wang Wenxian, Zhang Wei *et al. Journal of Alloys and Compounds*[J], 2018, 735: 1759

25 Li Yan, Wu Zhisheng. *Metals*[J], 2017, 7(4): 7040125

爆炸焊接镍/钢复合板界面的微观组织和力学性能

李　岩[1,2]，王贵成[1]，张文斌[1]，杨海娟[1]，李聚才[2]，刘翠荣[1,2]

(1. 太原科技大学 材料科学与工程学院，山西 太原 030024)

(2. 山西电子科技学院 智能制造产业学院，山西 临汾 041000)

摘　要：通过爆炸焊接技术制备了高性能的镍N6/45#钢复合板（N6/45#），通过金相显微镜（OM）、扫描电子显微镜（SEM）、电子背散射衍射（EBSD）以及力学性能测试，对界面及附近区域的微观组织进行了表征和分析，探讨了爆炸焊界面微观组织特征和力学性能特点。结果表明，沿着爆炸焊方向，N6/45#界面由平直结合逐渐演变为典型的波浪形结合，波峰和波谷处的晶粒具有高度的不均匀性，越靠近界面晶粒尺寸越小，在结合界面处发生了再结晶现象，形成了低应力变形带。纳米压痕试验发现界面结合区发生了塑形变形，波峰区域的纳米硬度值高于波谷区域。N6/45#界面抗拉伸强度为599.8 MPa，平均剪切强度达到了326.3 MPa，弯曲试验后N6/45#之间未发生分离现象。

关键词：爆炸焊接；镍N6/45#钢复合板；微观组织；纳米压痕

作者简介：李　岩，男，1988年生，博士，教授，太原科技大学材料科学与工程学院，山西 太原 030024，E-mail：2018023@tyust.edu.cn